Acta Montanistica Slovaca
ISSN 1335-1788
actamont.tuke.sk

Laboratory tests of unbound aggregate pavement base under cyclic loading and the impact of ground deformations caused by mining

Marcin GRYGIEREK[1], Piotr KALISZ[2], Magdalena ZIĘBA[3], Andrzej PYTLIK[4] and Witold FRĄC[5]*

Authors' affiliations and addresses:
[1] Silesian University of Technology, Faculty of Civil Engineering, Akademicka Street 5, Gliwice, Poland
e-mail: marcin.grygierek@polsl.pl

[2] Central Mining Institute, Department of Surface and Structures Protection, Gwarków Square 1, Katowice, Poland
e-mail: pkalisz@gig.eu

[3] Central Mining Institute, Department of Surface and Structures Protection, Gwarków Square 1, Katowice, Poland
e-mail: mzieba@gig.eu

[4] Central Mining Institute, Department of Mechanical Devices Testing and Rocks, Gwarków Square 1, Katowice, Poland
e-mail: apytlik@gig.eu

[5] Central Mining Institute, Department of Mechanical Devices Testing and Rocks, Gwarków Square 1, Katowice, Poland
e-mail: wfrac@gig.eu

***Correspondence:**
Magdalena Zięba, Central Mining Institute, Department of Surface and Structures Protection, Gwarków Square 1, Katowice, Poland
e-mail: mzieba@gig.eu
tel.: +48 32 259 21 09

Funding information:
Funding Agency: Polish Ministry of Science and Higher Education
Grant Number: 11142019-132 (in the Central Mining Institute)

How to cite this article:
Grygierek, M., Kalisz, P., Zięba, M., Pytlik, A. and Frąc, W. (2022). Laboratory tests of unbound aggregate pavement base under cyclic loading and the impact of ground deformations caused by mining. *Acta Montanistica Slovaca*. Volume 27 (1), 117-134

DOI:
https://doi.org/10.46544/AMS.v27i1.09

Abstract
The aim of the article is to determine the changes in the stiffness of an unbound aggregate base layer subjected to cyclic loading and the impact of mining deformation. The article presents the characteristics of the scale of changes in the stiffness of both the pavement layers and the subgrade for a category III mining area, i.e., for horizontal strains up to 6 mm/m. The characteristics are based on previous experience, which takes into account the impact of mining deformations that occurred in a category II mining area. The aim of the article was achieved based on the results of laboratory tests. These tests were conducted on a test stand that enables the simulation of the cyclic loading of the surface of a tested layer system and the horizontal strains of the ground. The cyclic loading caused by the rigid plate simulated the movement of vehicles. Numerical analysis of the issue for the conditions of laboratory tests was also carried out. This analysis was aimed at estimating the change in the parameters of individual layers in the tested system in subsequent stages of the laboratory tests. The results of the tests and analysis show that for horizontal tensile strains of 0.0–6.0 mm/m, a reduction in the elasticity moduli to approximately 35–45% for unbound aggregate and approximately 70% for fine-grained layers may occur.

Keywords
road pavement, static and cyclic loading, plate load test, mining area, horizontal strain, back calculation

Introduction

The unbound aggregate base is classified as a flexible layer and is very often used in road pavements. It plays a very important role in the distribution of loads on the pavement surface and determines the fatigue life of its mixed asphalt layers. A typical feature of this type of base is its susceptibility to permanent deformations from cyclic loads due to road traffic, which results in structural ruts on the pavement surface. Changes in the foundation conditions of unbound mix bases alter their mechanical properties. These changes most often result in an increase in pavement rut depth and a reduction in stiffness (a reduction in the modulus of elasticity). They then lead to an increase in tensile deformation at the bottom of the mixed asphalt layer and ultimately cause a reduction in pavement fatigue life.

The most common causes of subgrade deformation include the backfill subsidence of faulty sewer lines located relatively close to the subgrade base (Kuliczkowska, 2016) and changes in moisture both in the subgrade and the base (Rahman & Erlingsson, 2015; Rokitowski & Grygierek, 2017). An example of a special case is when a high groundwater table reaches the base (Rokitowski & Grygierek, 2017). These types of cases also include ground deformations in mining areas, which may cause both the loosening and compacting of the subgrade and layers built-in above it, including the base (Grygierek, 2018). The knowledge of the impact of these types of negative cases on the scale of changes in the stiffness of the unbound aggregate base is very important when it comes to pavement dimensioning, for example, in flooded areas. The mining area is a special case where the assessment of the impact of ground deformations on the pavement fatigue life and the structural rut depth is often essential.

This article presents the characteristics of the scale of changes in the stiffness of both the pavement layers and the subgrade based on previous experience. This experience includes the impact of mining deformations that occur in category II mining areas (Table 1) (Fig. 1). The aim of the article is to determine the scale of changes in the stiffness of an unbound aggregate base layer subjected to cyclic loading and the impact of deformation that occurs in category III mining areas. This aim was achieved based on the results of laboratory tests. These tests were conducted on a test stand that enables the simulation of the cyclic loading of the surface of a tested layer system and mining deformations. Numerical analysis, which aimed to estimate the change in the parameters of individual layers in the tested system during subsequent stages of the laboratory tests, was also carried out.

Tab. 1. Categories of mining areas in Poland

Category of mining area	Values of the surface deformation indices		
	Tilt T (mm/m)	Radius R of curvature K (km)	Horizontal strain ε (mm/m)
0	$T \leq 0.5$	$40 \leq \lvert R \rvert$	$\lvert \varepsilon \rvert \leq 0.3$
I	$0.5 < T \leq 2.5$	$20 \leq \lvert R \rvert < 40$	$0.3 < \lvert \varepsilon \rvert \leq 1.5$
II	$2.5 < T \leq 5$	$12 \leq \lvert R \rvert < 20$	$1.5 < \lvert \varepsilon \rvert \leq 3$
III	$5 < T \leq 10$	$6 \leq \lvert R \rvert < 12$	$3 < \lvert \varepsilon \rvert \leq 6$
IV	$10 < T \leq 15$	$4 \leq \lvert R \rvert < 6$	$6 < \lvert \varepsilon \rvert \leq 9$
V	$T > 15$	$\lvert R \rvert < 4$	$\lvert \varepsilon \rvert > 9$

The impact of mining deformations on road pavement, cases where there has been geometric changes in pavement in mining areas (Grygierek, 2018) and also the analysis of the mining subsidence trough are quite accurately described in the literature. The issue of mining impact on roads has been the subject of many research articles (Adelsohn et al., 2020; Deng, 2014; Grygierek, 2017; Grygierek & Kalisz, 2018; Gutierrez et al., 2010; Kay, 2012; Kotyrba & Kowalski, 2009; Lazecký et al., 2014; Nosenzo et al., 2013; Puertas, 2010; Swarbrick et al., 2015; Tong et al., 2014, 2016; Zha & Xu, 2019; Zhang et al., 2013). However, there is little in the literature concerning the scope of changes in the stiffness of the pavement layers and the subgrade. The knowledge available is connected with the results of observations and research conducted in Poland (Grygierek, 2018; Kawalec et al., 2019).

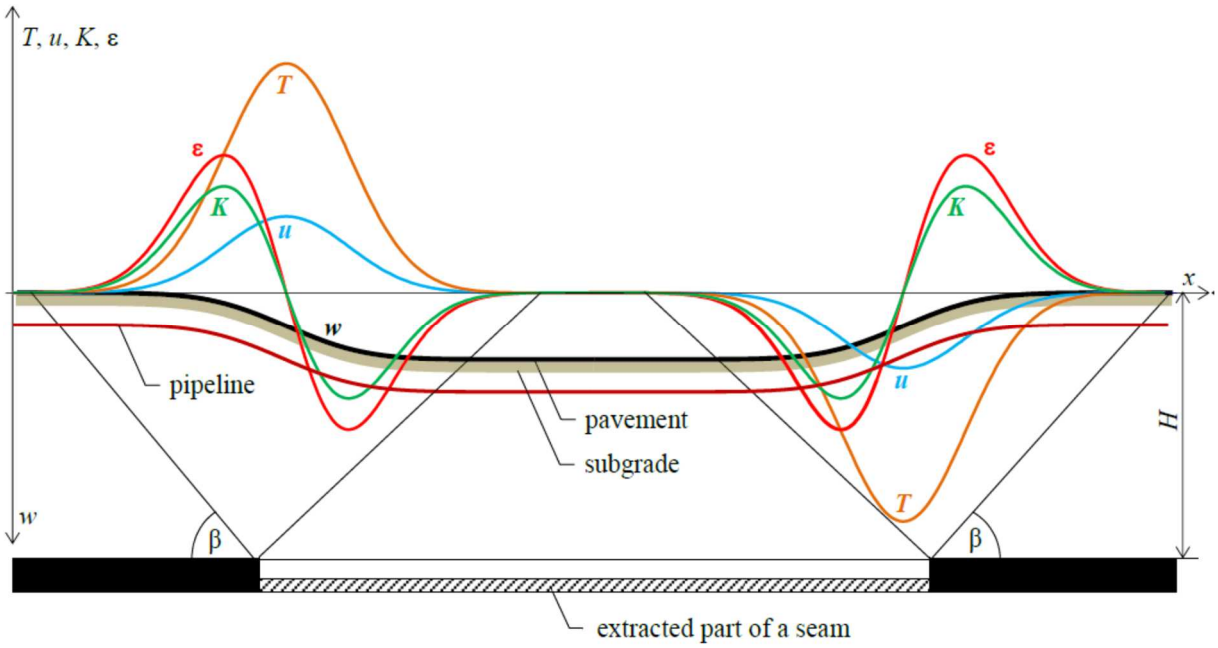

Fig. 1. The subsidence trough and the distribution of surface deformation indices according to the Knothe-Budryk theory (Kwiatek, 2007)*: w – subsidence, ε – horizontal strain, u – horizontal displacement, T – tilt, K – curvature; where: H – depth of extraction, β – the angle of draw*

Characteristics of changes in pavement mechanical properties due to ground deformation

When assessing the impact of underground mining on the pavement surface, the impact of both continuous and discontinuous deformations should be specified. In the case of discontinuous deformations (Fig. 2), the surface structure is assumed to be completely destroyed. When linear discontinuous surface deformations (LDSD) occur, sudden changes in the pavement surface are observed. These changes are accompanied by a significant reduction in the load-bearing capacity of the subgrade and the pavement layers built-in above it. Characteristic damage to a road pavement in LDSD areas is shown in Fig. 3. In the case of LDSD, the reduction in the modulus value of the unbound aggregate (modulus E_2 in Fig. 5) by up to 90% and the subgrade (modulus E_3 in Fig. 6) by 70% is observed. However, in the case of LDSD, the changes occur in a relatively short road section (Grygierek, 2017) of approximately 20 m. It is observed both in the distribution of pavement deflections and the modulus values. In the case of this type of pavement deformation, the complete repair of the pavement and its subgrade is essential. Figs. 4–6 show the distribution of the pavement deflections and the identified moduli of both the mix asphalt layer and the subgrade in the LDSD area.

Fig. 2. A sinkhole caused by shallow mining of zinc and lead ore in the area of the A1 motorway construction site, Poland

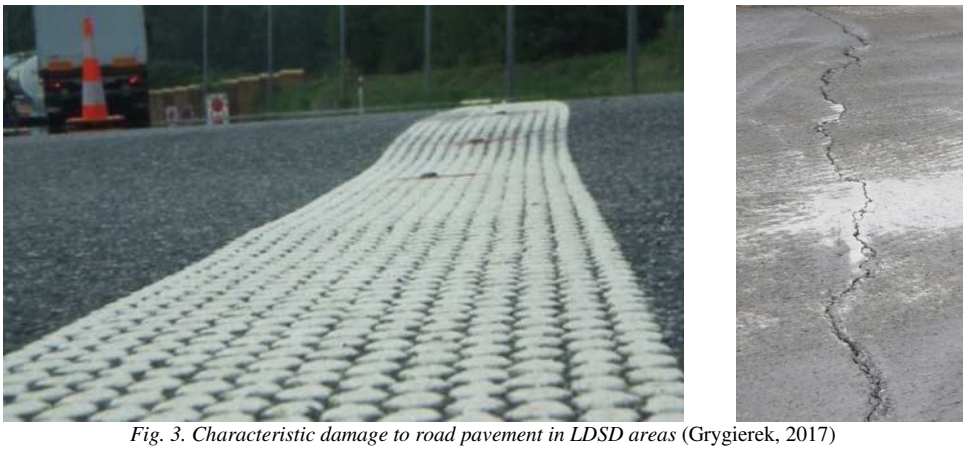

Fig. 3. Characteristic damage to road pavement in LDSD areas (Grygierek, 2017)

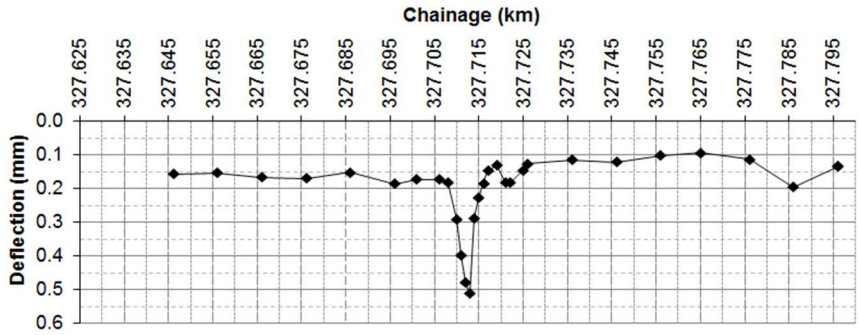

Fig. 4. Distribution of the pavement deflections in an LDSD area (Grygierek, 2017)

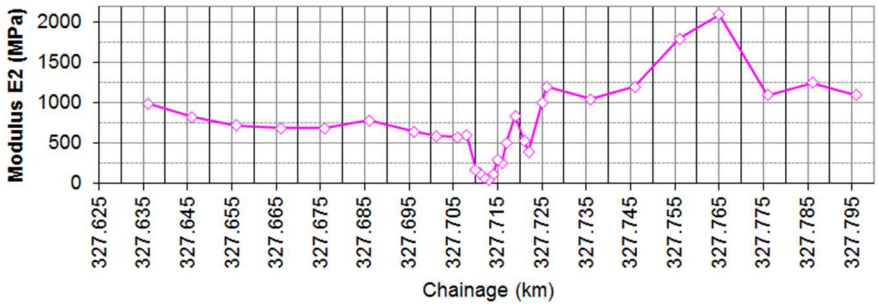

Fig. 5. Distribution of the identified moduli of the unbound aggregate E_2 (mix asphalt layer) in an LDSD area (Grygierek, 2017)

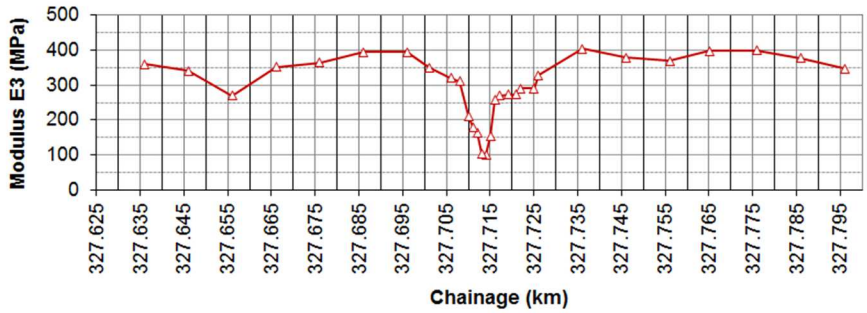

Fig. 6. Distribution of the identified moduli of the subgrade in an LDSD area (Grygierek, 2017)

In the case of continuous deformations, the pavement surface functions for many years. However, the damage and the reduction of its functionality due to the increase of ruts and cracks occur. Unlike discontinuous deformations, there are no such significant and sudden changes in road geometry. The experience presented in the research (Grygierek, 2010, 2018) (Figs. 7 and 8) shows that the modulus value of the unbound aggregate layers due to the impact of a horizontal tensile strain with a maximum value of 2.1 mm/m was reduced ΔE(-) by up to 45%. In the case of the pavement subgrade, the modulus value was reduced by approximately 25%. A characteristic feature of the analyzed pavement sections was the partial recovery of stiffness. This was probably caused by the movement of vehicles on the pavement and the end of mining impact on the surface. The

increase in the modulus value ΔE(+) after the end of the impact of horizontal tensile strain was approximately 18% for the aggregate and approximately 25% for the pavement subgrade. Such significant reductions in the modulus values are important for pavement fatigue life. The use of dependencies (1)–(4) in Figs. 7 and 8 are recommended in the range of horizontal tensile strains from 0.0 mm/m to 2.1 mm/m.

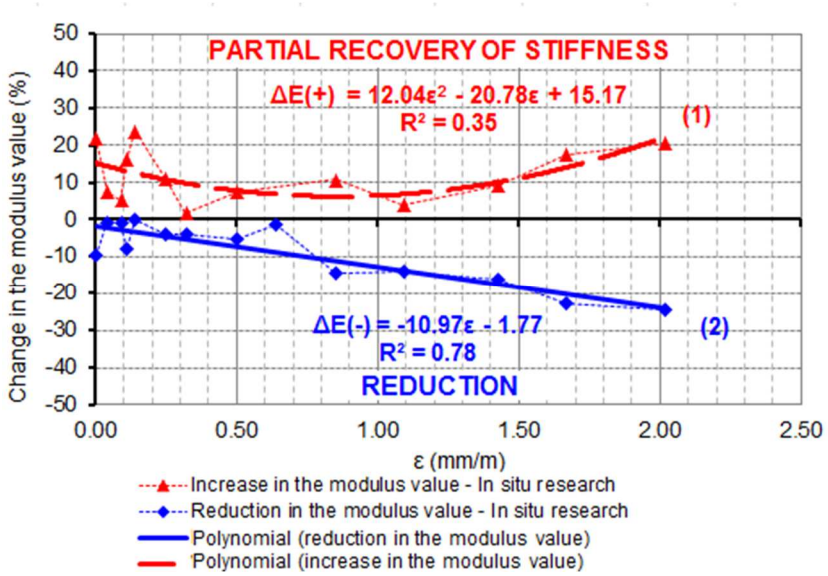

Fig. 7. Changes in the modulus values of the subgrade as a function of horizontal tensile strains (Grygierek, 2017)

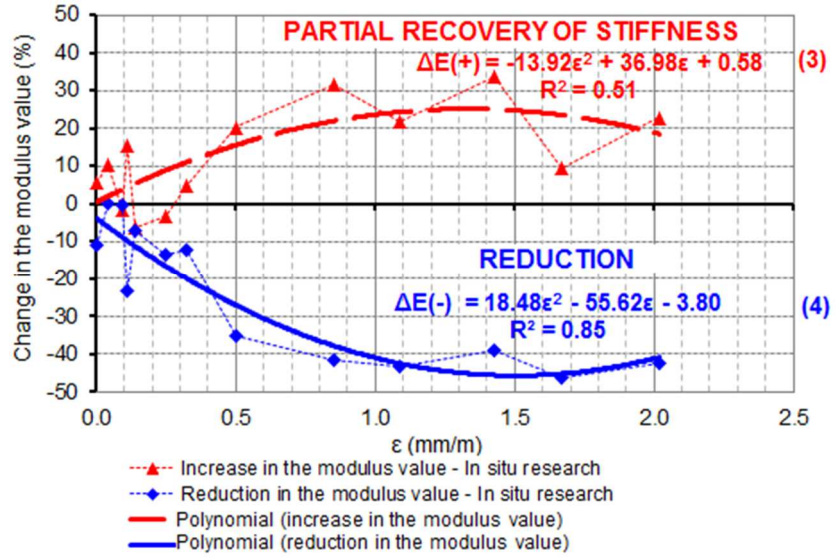

Fig. 8. Changes in the modulus values of the unbound aggregate layers as a function of horizontal tensile strains (Grygierek, 2017)

Laboratory tests

The laboratory tests were conducted on the test stand (Figs. 9 and 10), whose basic element is a rigid box with dimensions of 1.2 m x 1.0 m x 0.5 m. There are two immobile walls and two mobile walls in the test stand box. The mobile walls are perpendicular to the fixed walls (Fig. 10), and their displacement is forced with the use of horizontal actuators supported by stiff side frames. Their simultaneous movement simulates the impact of horizontal strains on the tested layer system. Moving mobile walls away from each other causes the horizontal loosening of the ground. The test stand enables the simulation of the cyclic loading of the surface of the tested layer system. This is the simulation of the impact of loads induced by heavy vehicles moving along the pavement surface. The hydraulic actuator, which is supported under the steel frame with a variable load induction system with the frequency of 0.35 Hz, was used to induce cyclic loading on the stiff circular plate of 200 mm diameter. Three sensors were used in the simulation to measure the vertical displacements of this plate. Standard static loading tests were also performed to determine the primary and the secondary deformation moduli. These tests were performed before and after cyclic loading and after the simulation of the horizontal soil strain impact on the layer system. The primary and secondary deformation moduli are the basic parameters used in road construction when checking the quality of layers.

The main goal of the conducted tests was to simulate both the cyclic loading of the tested layer system and the horizontal ground strains (Fig. 1) and also to measure the vertical displacement of the pressure plate.

The laboratory tests conducted on the test stand included the following stages:

- stage 1 – the preparation of a layer system: 30 cm of sand, 20 cm of unbound aggregate,
- stage 2 – the performance of the static loading test and the determination of the primary deformation modulus E_1 and the secondary deformation modulus E_2, and the deformation index E_2/E_1,
- stage 3 – the performance of the cyclic loading test of the layer system – 17,000 cycles at 450 kPa load in two steps,
- stage 4 – the performance of the static loading test and the determination of the primary deformation modulus E_1 and the secondary deformation modulus E_2, and the deformation index E_2/E_1,
- stage 5 – the simulation of the impact of horizontal tensile strains of 6.0 mm/m on the tested layer system,
- stage 6 – the performance of the static loading test and the determination of the primary deformation modulus E_1 and the secondary deformation modulus E_2, and the deformation index E_2/E_1,
- stage 7 – the performance of the cyclic loading test of the layer system – 10,000 cycles at 450 kPa load,
- stage 8 – the performance of the static loading test and the determination of the primary deformation modulus E_1 and the secondary deformation modulus E_2, and the deformation index E_2/E_1.

Stage 1

The tested layer system consisted of two layers: a lower layer of medium sand and an upper layer of unbound aggregate (dolomite) (Fig. 9). The preparation of the layer system began with the compaction of the medium sand layer of 30 cm thickness, using a mechanical compactor while maintaining optimum moisture of approximately 5%. The layer was compacted until the modulus tested on the layer system surface indicated a comparable value of the modulus after successive passes of the compactor. A lightweight deflectometer with a plate of 30 cm diameter was used to determine the modulus value. The compaction of the medium sand layer was completed to give the E_2 modulus value of approximately 60 MPa. The unbound aggregate layer of 20 cm thickness was compacted into three layers. After compaction, the modulus value, determined using a lightweight deflectometer, was approximately 80 MPa. After the preparation of the test stand, in order to ensure constant moisture of the tested layer system, its surface was covered with foil (Fig. 10).

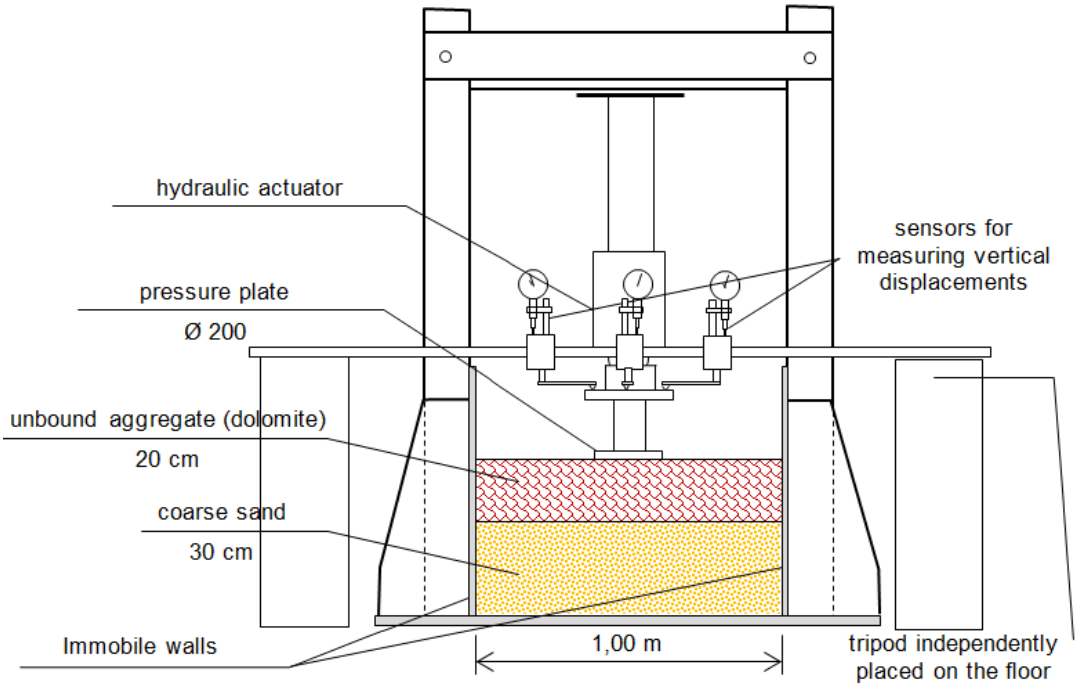

Fig. 9. Cross-section perpendicular to the immobile walls of the test stand with the prepared layer system

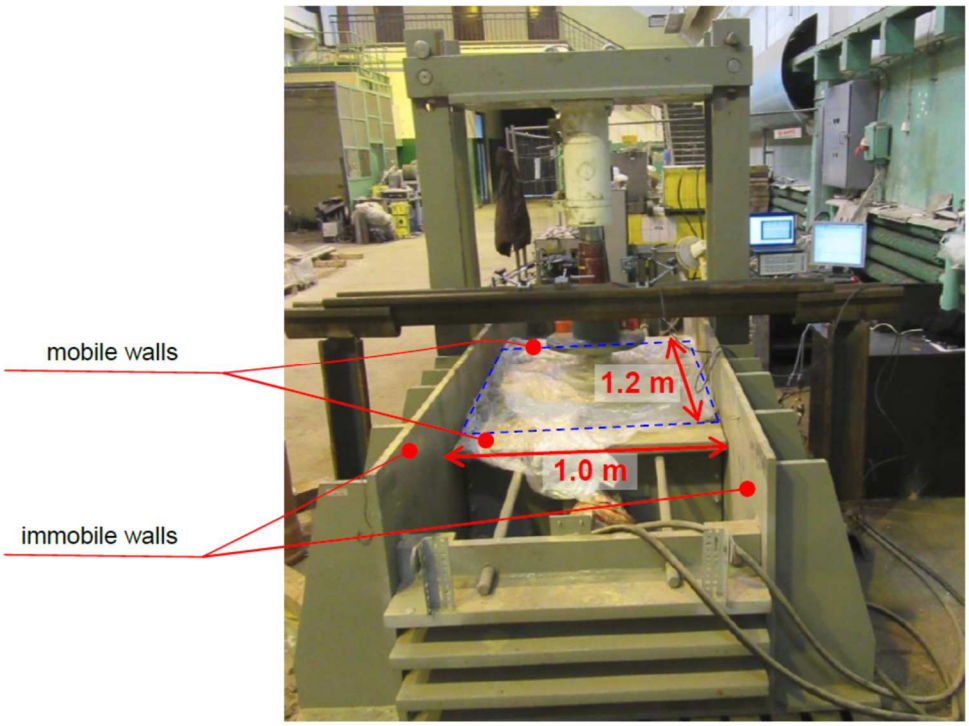

Fig. 10. The test stand with immobile sidewalls and mobile walls which are perpendicular to them

The grain size index (Cu) of the medium sand used in the laboratory tests was Cu=2.2 which classifies this sand as even soil (Cu<5), i.e., hard to compact. The aggregate was characterized by a grain size curve slightly exceeding the area of good grain size for a 0/31.5 grain base (Fig. 11) according to (The General Directorate for National Roads and Motorways, 2010). A mix with such grain size is widely used in road construction in Poland.

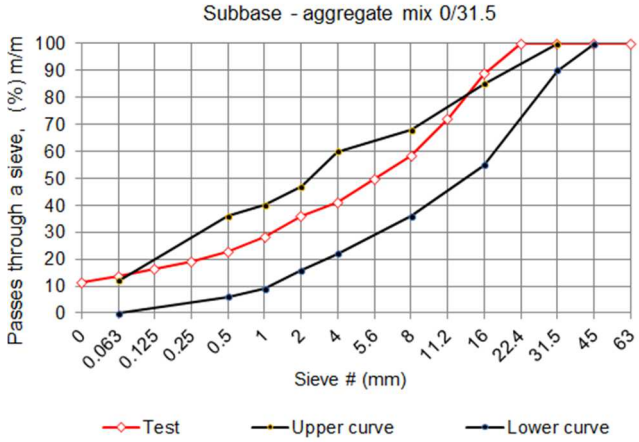

Fig. 11. Comparison of the grain size curves of the tested mix with the proper grain size curves for the subbase, where m/m is the weight ratio used in (The General Directorate for National Roads and Motorways, 2010)

Stage 2

The standard static loading test was conducted using a circular and stiff plate of 200 mm diameter. During the test, the vertical displacements of this plate were measured using subsequent load increments and decrements, i.e., 50 kPa, in the range from 0 kPa to 450 kPa (Fig. 17). The load was changed after the stabilization of vertical displacements, i.e., when the increase or decrease of vertical displacement was less than 0.05 mm/2 min. For each stage of the laboratory tests in which the static loading test was performed (stages: 2, 4, 6, and 8), the primary and secondary deformation moduli were determined (Table 2).

Stage 3

The purpose of the cyclic loading test was to simulate the impact of loads induced by heavy vehicles moving along the road pavement surface on the unbound aggregate layer. Finally, 17,000 cycles with a maximum amplitude of 450 kPa and a frequency of 0.35 Hz were applied in two steps – one 7,000 cycles and one 10,000 cycles. Fig. 12 presents the results of the first step of the cyclic loading test. In this stage, horizontal loading was not used. The unbound aggregate layer was subjected to the cyclic loading of the circular plate only.

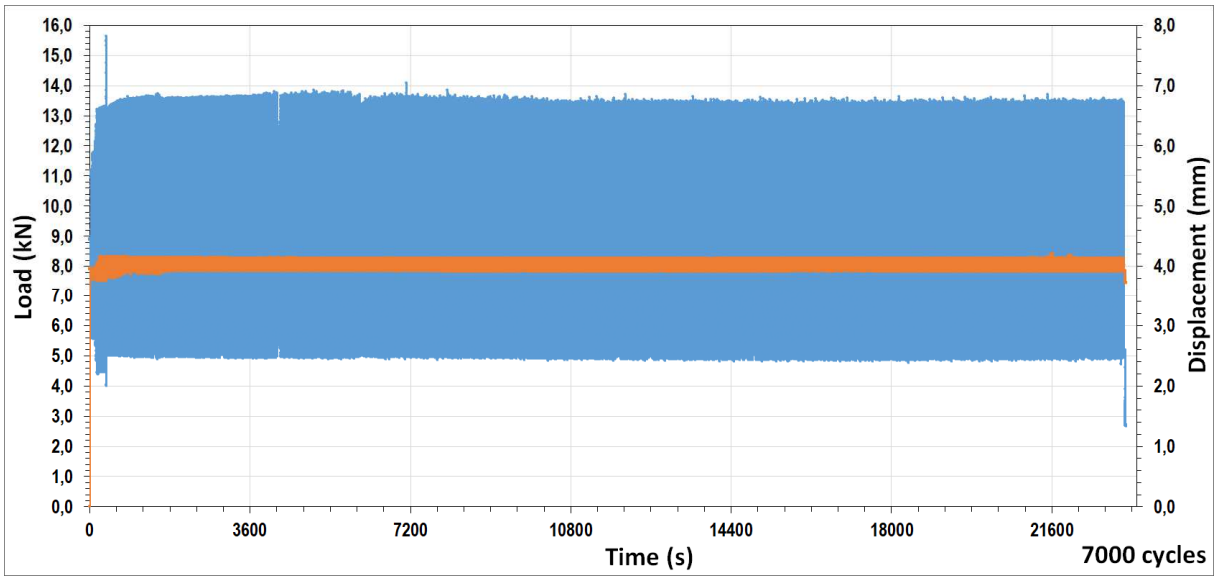

Fig. 12. Results of the first step of the cyclic loading test of 7,000 cycles, where load and displacement are marked blue and orange, respectively

Stage 4

The static loading test of the tested layer system was conducted according to the same principles as in stage 2 (Fig. 17) (Table 2).

Stage 5

The impact of horizontal tensile strains (Fig. 1) was simulated by the simultaneous movement of the mobile walls of the test stand box (Fig. 10). Horizontal strains, among all the surface deformation indices (Fig. 1), have the most negative impact on the reduction in stiffness of both the subgrade and the pavement layers. Each mobile wall was moved outside by 3.5 mm, which enabled the simulation of the impact of horizontal strains of ε=6.0 mm/m (2x3.5 mm/1.20 m) on the tested layer system. This value of the horizontal strains corresponds to the upper range of a category III mining area (Table 1). After the movement of the walls, a crack was observed on the surface of the unbound aggregate layer. The course of the crack was perpendicular to the direction of the movement of the walls (Fig. 13). The maximum crack width did not exceed 2 mm.

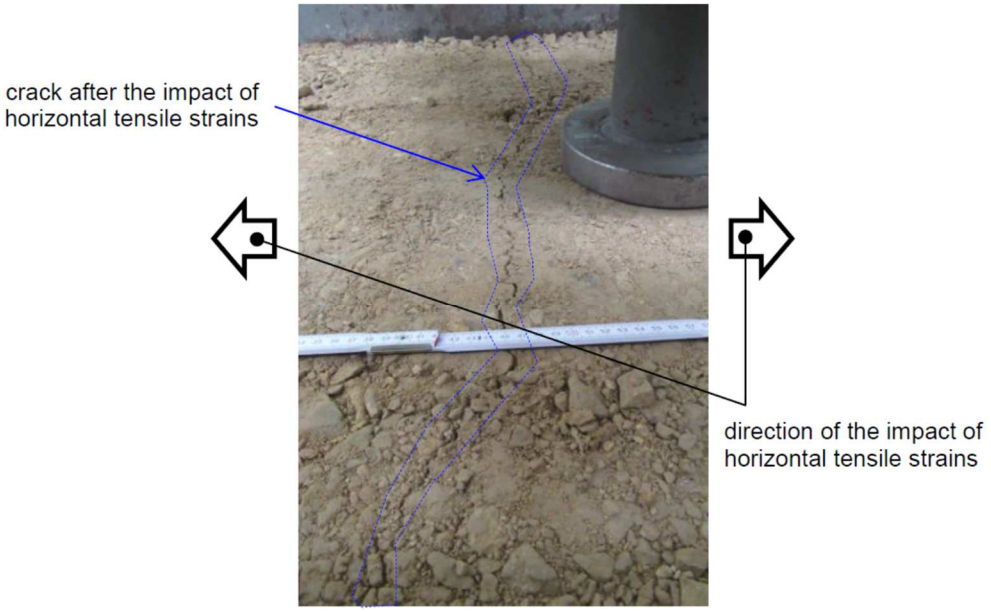

Fig. 13. Crack on the surface of the tested layer system after the impact of horizontal tensile strains of 6.0 mm/m

Stage 6

The static loading test of the tested layer system was conducted according to the same principles as in stages 2 and 4 (Fig. 17) (Table 2).

Stage 7

After the impact of horizontal tensile strains of ε = 6.0 mm/m, the cyclic loading test of the tested layer system was performed for the same conditions as in stage 3. Finally, 10,000 cycles with a maximum amplitude of 450 kPa and a frequency of 0.35 Hz were applied. Fig. 14 presents the results of the cyclic loading test after the impact of horizontal tensile strains on the layer system.

After the cyclic loading test, the widening of the crack (Fig. 13) on the surface of the unbound aggregate layer was inventoried. The width of the crack increased from 2 mm to 4 mm (marked blue in Fig. 15). A new crack of relatively small width was recorded on the surface of the unbound aggregate layer, on the other side of the pressure plate (marked red in Figs. 15 and 16).

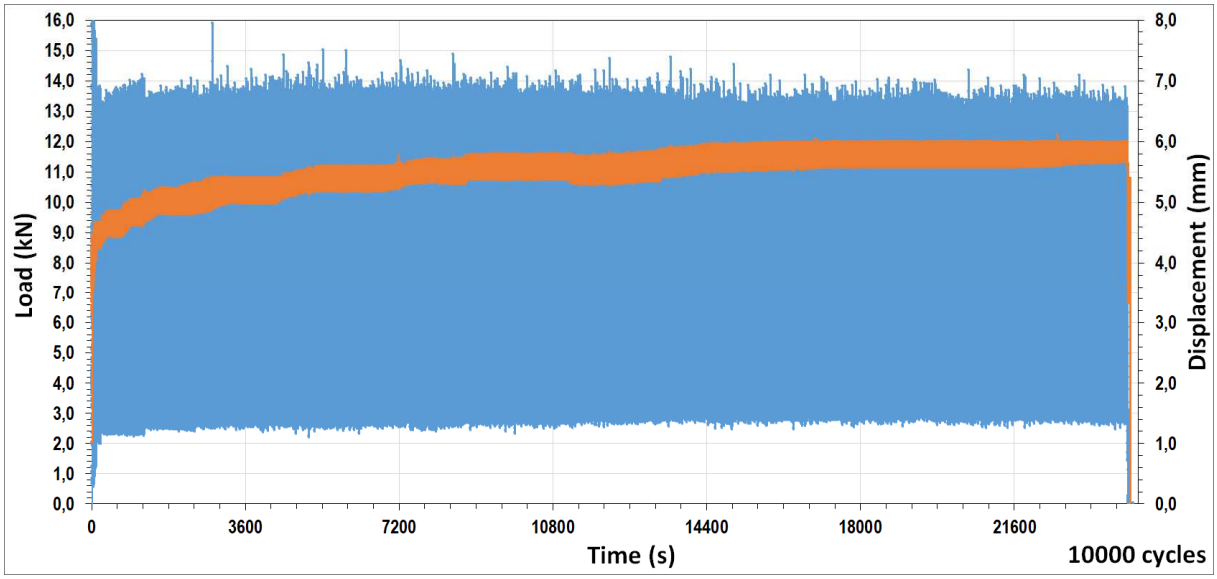

Fig. 14. Results of the cyclic loading test after the impact of horizontal tensile strains on the tested layer system, where load and displacement are marked blue and orange, respectively

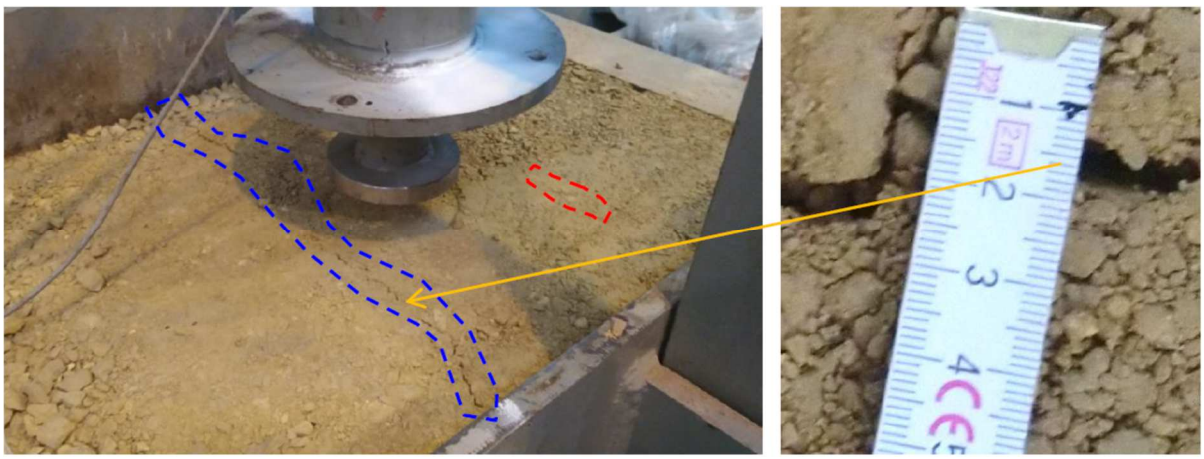

Fig. 15. The surface of the layer system after the impact of horizontal tensile strains and the cyclic loading test of 10,000 cycles

Fig. 16. A new crack on the surface of the aggregate layer after the impact of horizontal tensile strains and the cyclic loading test of 10,000 cycles

Stage 8

The static loading test of the tested layer system was conducted according to the same principles as in stages 2, 4, and 6. Fig. 17 presents the results of the static loading tests of the tested layer system at various stages, i.e., 2, 4, 6, and 8.

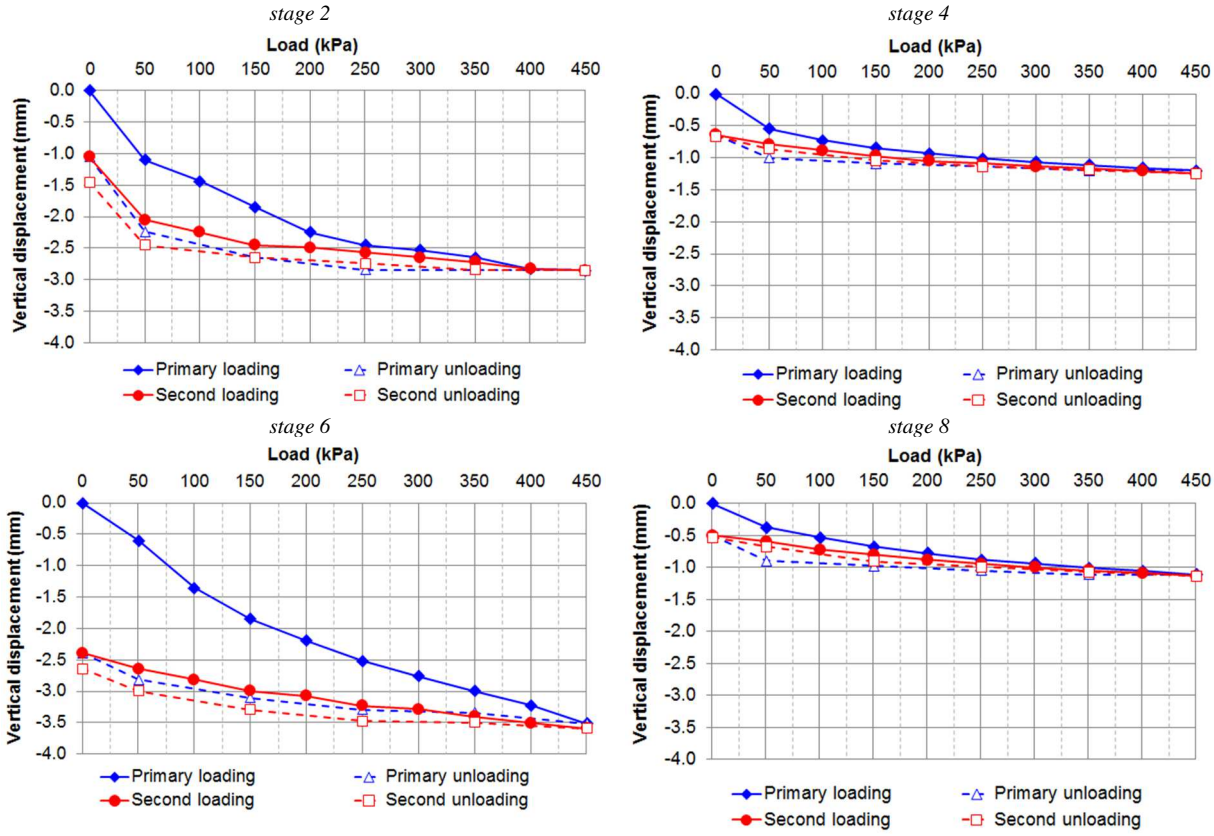

Fig. 17. Results of the static loading tests of the tested layer system at various stages

After the static loading tests, the depth of permanent deformation on the contact surface between the pressure plate and the tested unbound aggregate layer was visually assessed (Table 2). The subsidence of the pressure plate at various stages, i.e., 4, 6, and 8, is shown in Fig. 18.

Tab. 2. Results of the static loading tests of the tested layer system

	Stage						
	2	3	4	5	6	7	8
	Static loading test	Cyclic loading tests, 17,000 cycles	Static loading test	The impact of horizontal tensile strains of 6.0 mm/m	Static loading test	Cyclic loading test, 10,000 cycles	Static loading test
Total permanent deformation (mm)	2.8	6.8	8.1	-	11.6	17.3	18.4

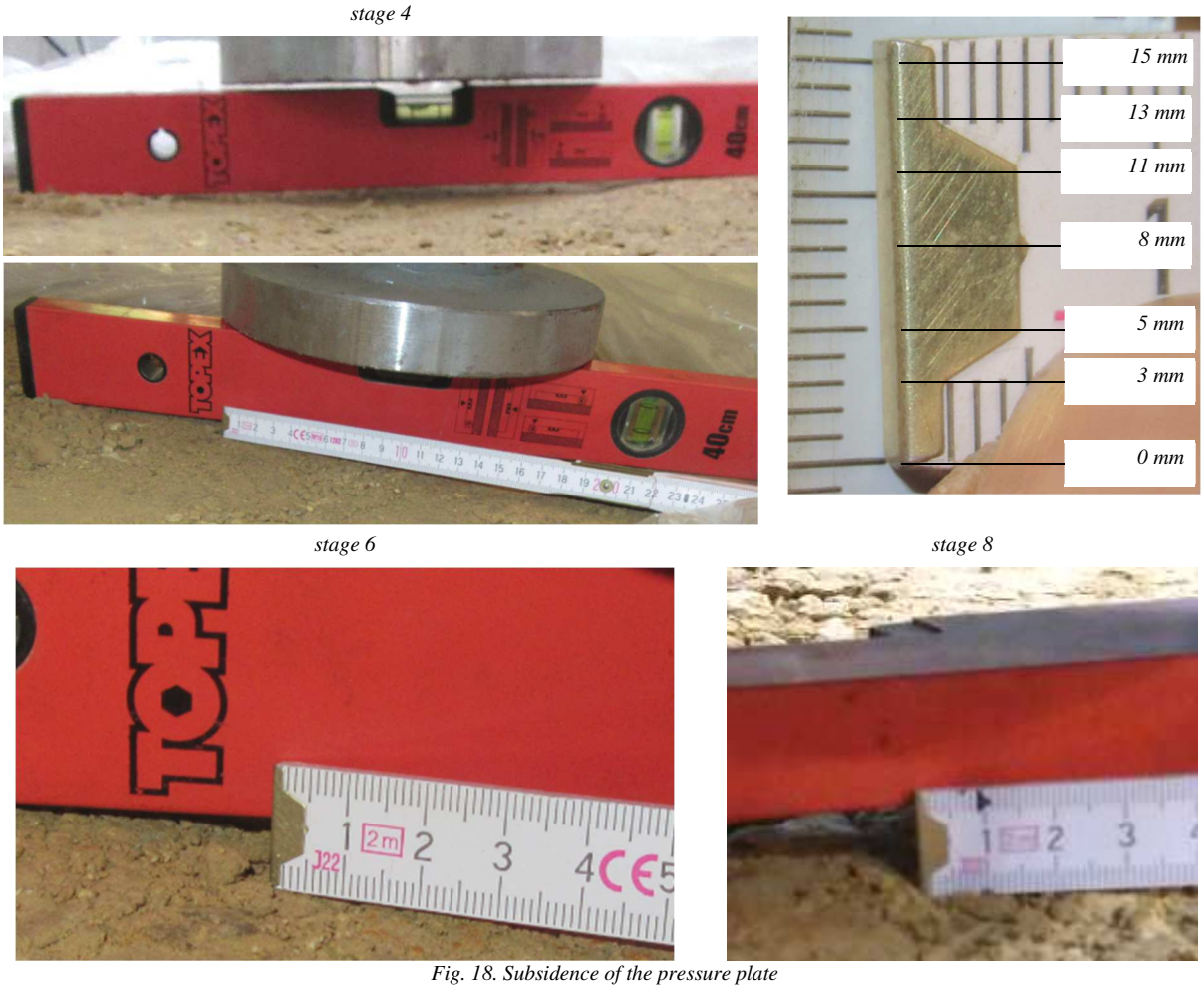

Fig. 18. Subsidence of the pressure plate

Numerical analysis

The numerical analysis aimed to estimate the change in the values of the parameters of individual layers during subsequent stages of the tests. The elastic model was used in the numerical analysis. Poisson's ratio was assumed to be 0.3, and the modulus of elasticity E values were determined based on the back-calculation. A load range from 0 kPa to 250 kPa was considered because, with a higher load range, the effect of bottom stiffness was observed on the distribution of vertical displacements. Assuming the value of 250 kPa as the upper load limit in the back analysis of moduli, the values of the secondary deformation modulus were used. These values reach values similar to the constant (stage 2, stage 4, and stage 8) after exceeding approximately 250 kPa (Fig. 21). This effect is seen in the partial load being taken over by the rigid bottom, as well as by the walls of the test stand, and thus lower vertical displacements. Moreover, in the inverse calculations, it was considered sufficient to use a minimum of 6 points to describe the relationship: load - displacement, i.e., 0 kPa, 50kPa, 100 kPa, 150 kPa, 200 kPa, 250 kPa. The calculations for a three-dimensional model (Fig. 19) were conducted in the Z_Soil 11.03 program (Z_Soil 2011). The estimation of the values of the parameters of the model consisted of finding such values of the modulus of elasticity of both of the layers so that the values of vertical displacements calculated in the model and measured during the laboratory tests were as close as possible to reality (Fig. 20). The parameters were determined for the static measurements in stages 2, 4, 6, and 8. The results of the back calculations are presented in Table 3. The calculations were performed by the iterative method, which aimed to obtain the highest possible value of the determination coefficient R^2 according to formula 1

$$R^2 = 1 - \frac{\sum\left(s_i^E - s_i^T\right)^2}{\sum\left(s_i^E\right)^2 - \frac{\left(\sum s_i^E\right)^2}{n}} \tag{1}$$

where:

n – the number of data points,

s_i^E – vertical displacement of the circular and stiff plate measured during the laboratory tests,
s_i^T – vertical displacement (theoretical) calculated in the FEM model.

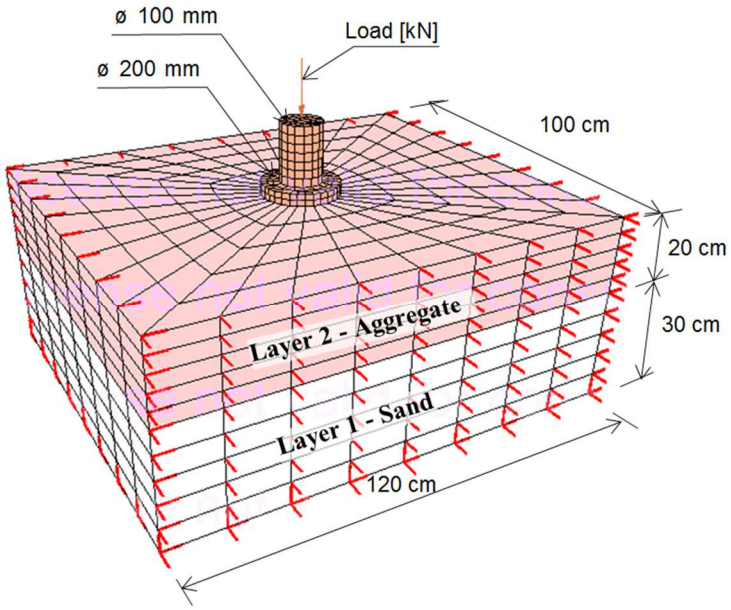

Fig. 19. Numerical model

Tab. 3. Results of the back calculations

	Stage			
	2	4	6	8
	Static loading test	Static loading test, after the cyclic loading tests, 17,000 cycles	Static loading test, after the impact of horizontal tensile strains of 6.0 mm/m	Static loading test, after the cyclic loading test, 10,000 cycles
	Resilient modulus (MPa)			
Aggregate 0/31.5	15	70	45	69
Sand	8	33	10	33
R^2	0.70	0.94	0.96	0.98

stage 2

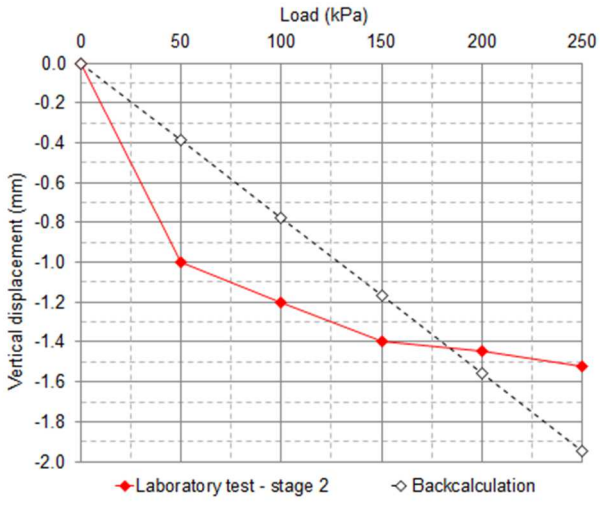

stage 4

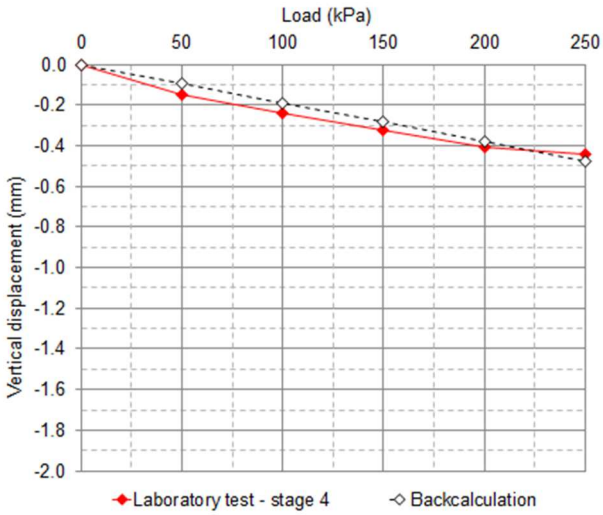

stage 6

stage 8

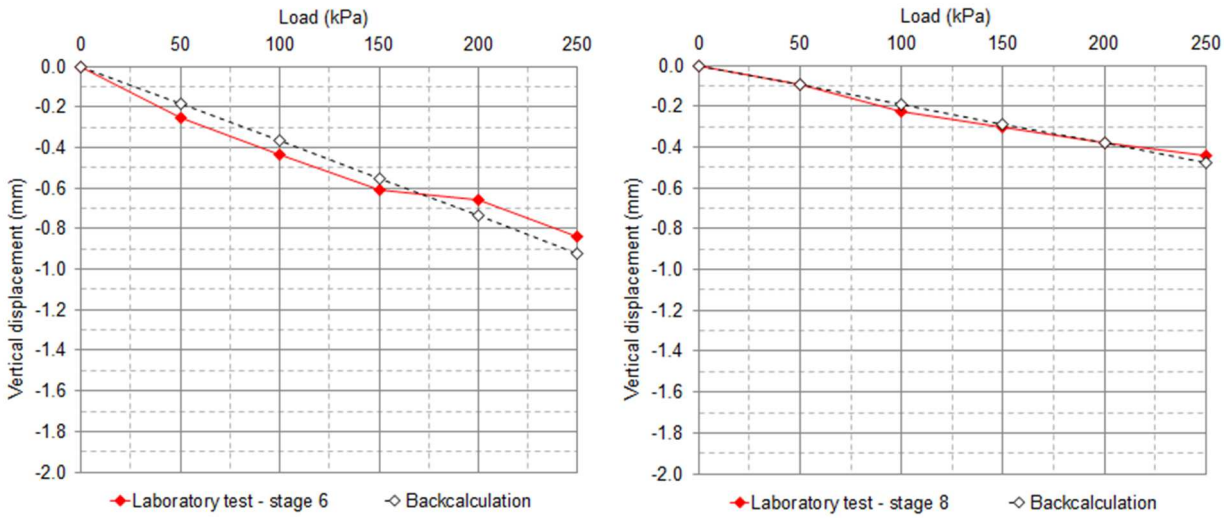

Fig. 20. The results of fitting the theoretical and measured vertical displacements

Discussion and results analysis

General discussion

The measurement of vertical displacements under the static plate loading was adopted as the basic test for assessing the properties of the tested layer system. A plate of 200 mm diameter was used to meet the condition of the minimum width of the test stand in relation to the plate diameter loading the tested layer system. Compliance with this condition enabled the assumption that the horizontal dimensions of the test stand did not have a significant effect on the distribution of stress in the tested layer system. However, when analyzing the measured vertical displacements (Fig. 17), decreasing displacement in the primary loading (marked blue in Fig. 17) increases in the successive second loading stages (marked red in Fig. 17), which indicates the strengthening of the tested layer system. This may be due to the increasing influence of the rigid floor under the test stand. The effect of the influence of the rigid floor is not observed in stages 2 and 6. In stage 2, the layers were not yet fully compacted, and in stage 6, the test was performed after the impact of horizontal tensile strains on the layer system. This effect is visible in the results of stage 4 (Fig. 21), where the secondary deformation modulus (formula 2), calculated for the load range of 200–300 kPa and subsequent load ranges, reaches similar modulus values (on average 190 MPa).

$$E_{1,2}^{(p_1,p_2)} = 0{,}75D\,\frac{\Delta p}{\Delta s} \tag{2}$$

where:

E_1, E_2 – primary and secondary deformation modulus, MPa,

Δp – load increase during the primary and secondary loading, MPa,

Δs – displacement corresponding to the assumed load range during the primary and secondary loading, i.e. between 100–200 kPa, mm,

D – plate diameter, D = 200 mm.

The results of the static loading tests of the layer system (primary deformation modulus E_1 and secondary deformation modulus E_2, and deformation index I_o) for the assumed load range of 100–200 kPa are presented in Table 4.

Tab. 4. Results of the static loading tests of the layer system in individual stages for the assumed load range 100–200 kPa

	Stage			
	2	4	6	8
Parameter	Static loading test	Static loading test, after the cyclic loading tests, 17,000 cycles	Static loading test, after the impact of horizontal tensile strains of 6.0 mm/m	Static loading test, after the cyclic loading test, 10,000 cycles
E_1 (MPa)	18.5	73.2	23.1	62.5
E_2 (MPa)	61.2	88.2	85.7	96.8
$I_o = E_2/E_1$	3.38	1.21	3.71	1.55

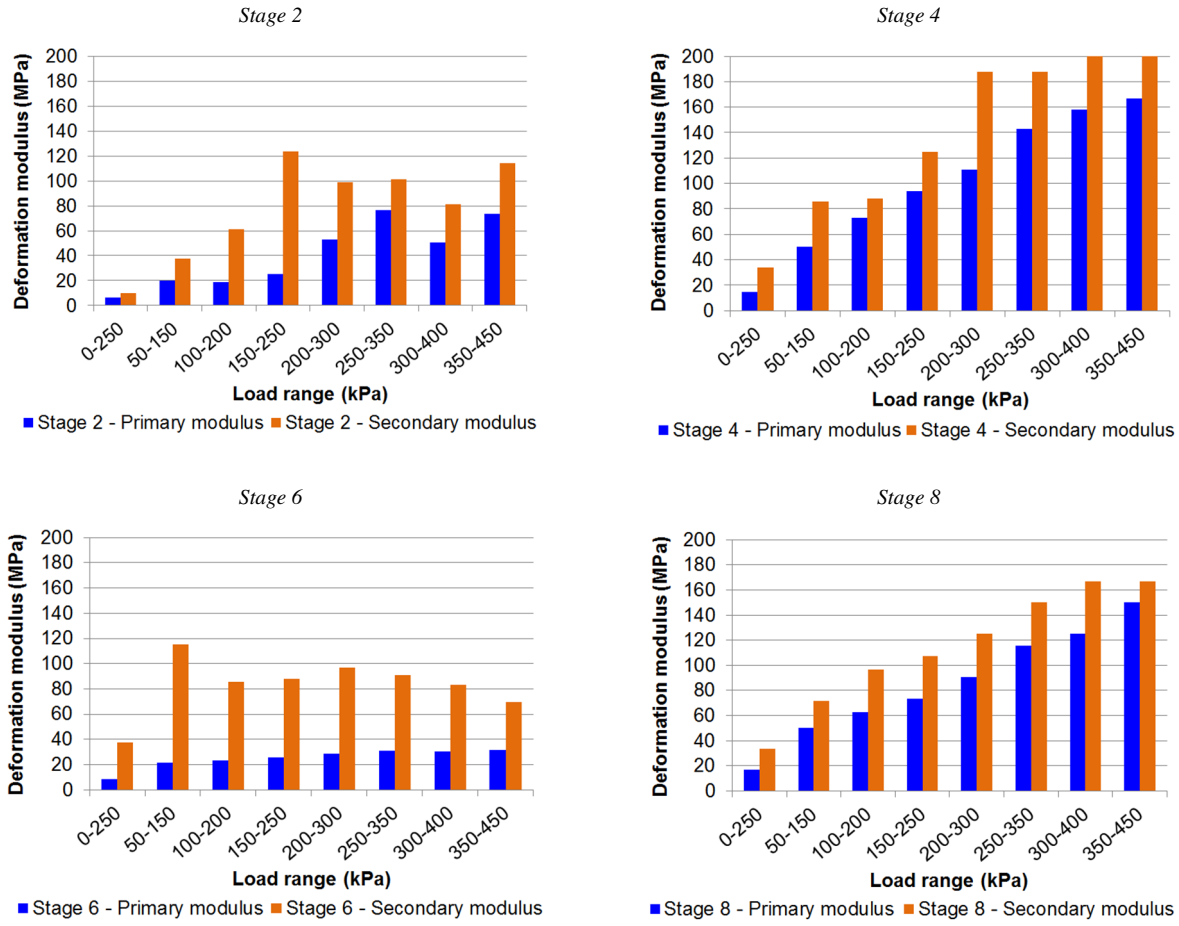

Fig. 21. Distribution of the primary and secondary deformation modulus for various load ranges in individual stages of the static loading tests

Analysis of changes in the stiffness of the layer system

The tests results enabled both the assessment of changes in the deformation modulus describing the stiffness of the full layer system and the assessment of the behavior of individual layers using elasticity moduli. The values of both parameters are determined by the impact of the boundary conditions of the test stand and the quality of the compaction of the layer system in stage 1. Taking into account the indicated limitations, the values of measured displacements in the following ranges of pressure applied on the surface were used in assessing the behavior of the layers: 100–200 kPa in the case of deformation moduli (Fig. 22) and 0–250 kPa in the case of back-calculation and elasticity moduli (Fig. 20). The values of the elasticity moduli from the first test (stage 2) were not analyzed.

Elasticity moduli of both layers after load simulation (stage 3) reached values of 70 MPa (aggregate) and 33 MPa (sand). The sand was even-grained, so its modulus of elasticity was low. The modulus of the aggregate layer, which was compacted on the top of the sand, also did not reach a high value. However, the modulus of elasticity was strongly dependent on the foundation conditions of this layer, i.e., it depended on the stiffness of the sand. This observation confirms formula 3 describing the non-linear characteristics of the unbound mix modulus in the function of the substrate modulus (Claessen et al., 1977; Judycki et al., 2017). Formula 3 shows that in the case of the subgrade layer characterized by the modulus value of 33 MPa, the modulus of the built-in layer on it should be approximately 72 MPa.

$$E_{ua} = k\ E_o \tag{3}$$

where:

E_{ua} – modulus of elasticity of the unbound aggregate layer,
k – $k = 0.2\ h^{0.45}$,
h – thickness of the calculated layer, (mm),
E_o – modulus of elasticity of the subgrade under the layer for which the modulus of elasticity is calculated.

After simulating the load on the layer system, the secondary deformation modulus reached 88 MPa (Table 4). According to the experience of road design in Poland, it meets the requirements of the subgrade of upper pavement course for the lowest categories of traffic class – KR1–KR2 (Judycki et al., 2013, 2017). An I_o index of 1.2<2.0 indicates good compaction of the tested layer system. In the next stage (stage 5), the tested layer system was subjected to the impact of horizontal tensile strains. The simulated strains of ε = 6.0 mm/m correspond to the horizontal tensile strains of a category III mining area (Table 1). The results of static loading (stage 6) performed after the impact of the horizontal tensile strains indicate a significant reduction in the stiffness of both layers. Comparing the value of the secondary deformation modulus before deformation (88.24 MPa – stage 4) to the primary deformation modulus after deformation (23.1 MPa – stage 6), a reduction in the value of about 73% is observed. At the secondary loading (stage 6), the modulus increased to a value close to that of before the impact of the horizontal tensile strains. However, the values of the secondary deformation modulus for all pressure increase (Fig. 21 – stage 6), and these values are close to a constant value. Comparing such a distribution to these of stages 4 and 8 indicates that the boundary conditions of the test stand do not affect the calculation result. This fact may be explained by the loosening of the layers in relation to the situation after subjecting the layer system to cyclic loads. The effect of the loosening of the layers is also observed in the values of elasticity moduli (Table 3) (Fig. 23), which were reduced by approximately 36% in the case of aggregate and by approximately 70% in the case of sand. These are very significant reductions in the values of moduli. However, when comparing them to the experience of field tests (Fig. 7 – subgrade and Fig. 8 – aggregate), the results of laboratory tests confirm observations from previous experiences. For the aggregate layer (Fig. 24), a significant modulus reduction to about 42% is observed in the strain range of 0.0–1.25 mm/m. Further increase in horizontal tensile strains, i.e., from 1.25 mm/m to 6.00 mm/m, do not cause such a significant reduction in the modulus value. Taking into account previous experience and the results of laboratory tests, it can be argued that the reduction of the aggregate elasticity modulus is approximately 35–45% in the range of horizontal strains from approximately 1.25 mm/m to approximately 6.00 mm/m and is close to a constant value. The distribution of moduli reduction is slightly different in the case of layers of fine-grained materials that occur in the pavement subgrade. In this case, the results of field tests indicate a linear increase in the reduction in the strain range from 0.0 mm/m to 2.0 mm/m (Fig. 7). The results of laboratory tests confirm this relationship (Fig. 25). The different distribution of changes in moduli values for fine-grained materials (for example, sand) and materials with typical particle size for the layers of base and subbase (aggregate, for example, 0/31.5, 0/63) is related to the grain size and the resulting angle of internal friction. Stage 7, in which the tested layer system was again subjected to cyclic loadings, enabled the recovery of the stiffness of the tested layer system. This is indicated by the results of the tests conducted in stage 8. Both in the case of elasticity moduli (Fig. 23) and deformation moduli (Fig. 22), values comparable to those identified in stage 4 (i.e., after the simulation of the layer loading in stage 3) and before the loosening of the layers (stage 5) were obtained. Considering the fact that cyclic loadings were applied directly to the layer of the unbound mix, these layers were very effectively compacted as they are during technological works. The obvious consequence of recovering the stiffness of the layers was a significant increase in permanent deformations expressed by vertical deformation (Table 2), approximately 6 mm between the end of the tests in stages 4 and 8.

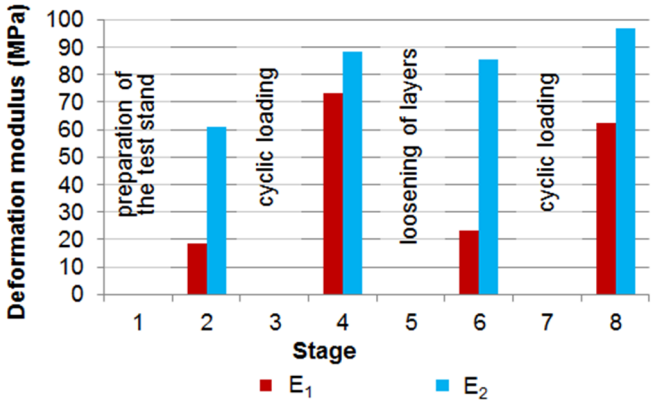

Fig. 22. Distribution of the primary (E_1) and secondary (E_2) deformation modulus in the individual stages of the test (pressure range 100–200 kPa)

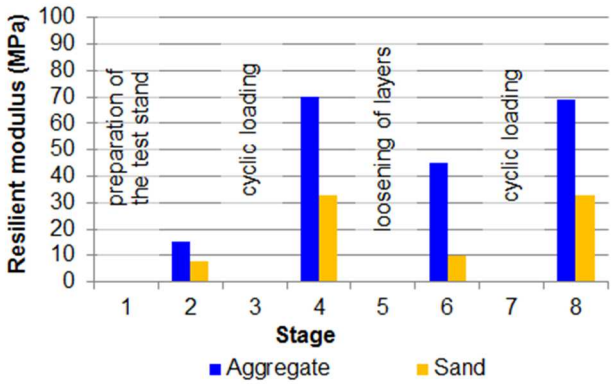

Fig. 23. Distribution of the elasticity (resilient) moduli of the layers of the tested system according to (Table 3)

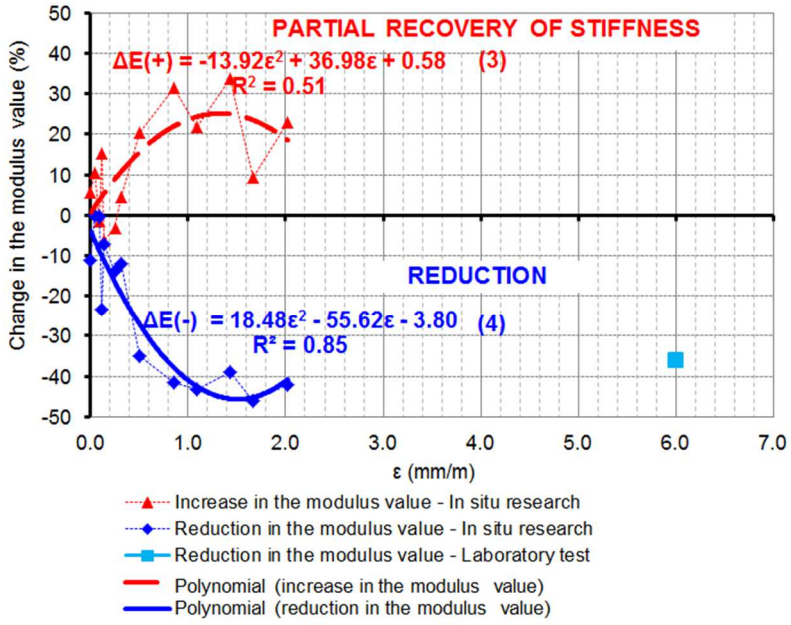

Fig. 24. Changes in the modulus values of the unbound aggregate layers as a function of horizontal loosening strains – according to the field and laboratory tests

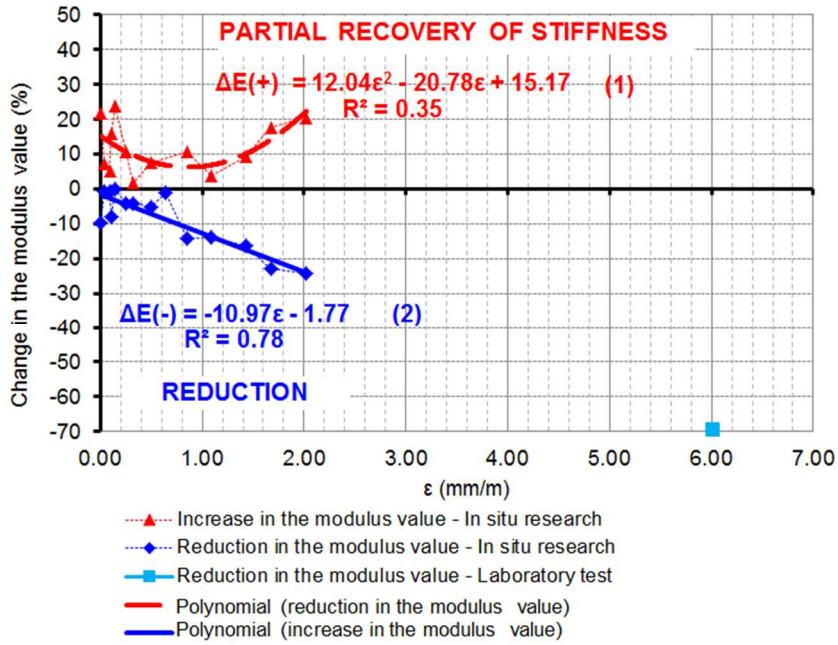

Fig. 25. Changes in the modulus values of the subgrade as the function of horizontal tensile strains – according to the field and laboratory tests

Conclusions

There are many causes of subgrade deformation under an aggregate base, including ground deformations in mining areas. Knowledge of the impact of these types of negative cases on the scale of changes in the stiffness of the unbound aggregate base is very important in the aspect of pavement dimensioning. The aim of this article is to determine the scale of changes in the stiffness of the unbound aggregate base layer subjected to cyclic loading and the mining impact of a category III mining area. This aim was achieved based on the results of laboratory tests.

Under cyclic loading, the further compaction of unbound aggregate layers is observed. The range of the compaction and the accompanying depth of permanent deformation (rut) depends on the properties of the material used and the initial compaction of the layer.

If the impact of the horizontal tensile strains of the subgrade under the aggregate layer occurs, the stiffness of this layer is significantly reduced and is recovered with each subsequent load. The analogy of the cyclic loadings during the laboratory tests to the cyclic loadings of the pavement layer system with vehicle traffic of variable frequency – depending on the traffic volume and the axle configuration of heavy vehicles – was used.

The results of the conducted laboratory tests indicate that under the impact of horizontal tensile strains on the subgrade, changes in the structure of the aggregate layer in the form of cracks may occur. This corresponds to the field observations. These cracks can significantly affect the local reduction in the stiffness of this layer, as evidenced by the results of calculated deformation moduli. In the aggregate, in the strain range of 0.0–1.25 mm/m, a significant modulus reduction to approximately 42% is observed. Further, an increase in horizontal tensile strains (ε=1.25–6.00 mm/m) does not cause such a significant reduction in the modulus value. The reduction of the value of elasticity moduli of fine-grained medium (sand) is linear in the range of horizontal tensile strains from 0.0 mm/m to 6.0 mm/m. The laboratory and field research results show that for horizontal tensile strains of 0.0–6.0 mm/m, the reduction in the elasticity moduli to approximately 35–45% for unbound aggregate and approximately 70% for fine-grained layers may occur. These are qualitative conclusions and require further research and analysis, although they can already be used in the assessment of phenomena related to the impact of mining deformations on the stiffness of road pavement layers.

References

Adelsohn, E., Iannacchione, A., & Winn, R. (2020). Investigations on longwall mining subsidence impacts on Pennsylvania highway alignments. International Journal of Mining Science and Technology, 30(1), 85–92. https://doi.org/10.1016/j.ijmst.2019.12.012.

Claessen, A., Edwards, J. M., Sommer, P., & Uge, P. (1977). Asphalt Pavement Design - the Shell Method. Volume I of Proceedings of 4th International Conference on Structural Design of Asphalt Pavements, Ann Arbor, Michigan, August 22-26, 39–74.

Deng, W. N. (2014). Research on allowable deformation of highway influenced by coal mining subsidence. In Advanced Materials Research (Vols. 962–965, pp. 1165–1168). https://doi.org/10.4028/www.scientific.net/AMR.962-965.1165.

Grygierek, M. (2010). Zmienność modułów sprężystości niezwiazanych warstw nawierzchni drogowej w warunkach górniczych odkształceñ rozluźniajacych. Drogi i Mosty, 2, 17–30.

Grygierek, M. (2017). Change in stiffness of pavement layers in the linear discontinuous deformation area. IOP Conference Series: Materials Science and Engineering, 245(4), 042051. https://doi.org/10.1088/1757-899X/245/4/042051.

Grygierek, M. (2018). Problematyka funkcjonowania dróg na terenach górniczych. Magazyn Autostrady, 1–2, 40–45.

Grygierek, M., & Kalisz, P. (2018). Influence of mining operations on road pavement and sewer system – selected case studies. Journal of Sustainable Mining, 17(2), 56–67. https://doi.org/10.1016/j.jsm.2018.04.001.

Gutierrez, J. J., Vallejo, L. E., & Lin, J. (2010). A Study of Highway Subsidence due to Longwall Mining using data collected from I-79. In Report.

Judycki, J., Jaskuła, P., Pszczoła, M., Alenowicz, J., Dołżycki, B., Jaczewski, M., Ryś, D., & Stienss, M. (2013). Katalog typowych konstrukcji nawierzchni podatnych i półsztywnych.

Judycki, J., Jaskuła, P., Pszczoła, M., Ryś, D., Jaczewski, M., Alenowicz, J., Dołzycki, B., & Stienss, M. (2017). New polish catalogue of typical flexible and semi-rigid pavements. MATEC Web of Conferences. https://doi.org/10.1051/matecconf/201712204002.

Kawalec, J., Grygierek, M., Koda, E., & Osiński, P. (2019). Lessons learned on geosynthetics applications in road structures in Silesia mining region in Poland. Applied Sciences (Switzerland), 9(6). https://doi.org/10.3390/app9061122.

Kay, D. (2012). Managing mine subsidence along railways and highway pavements in the southern coalfield. In Australian Geomechanics Journal (Vol. 47, Issue 1, pp. 33–52).

Kotyrba, A., & Kowalski, A. (2009). Linear discontinuous deformation of A4 highway within mining area "Halemba". Gospodarka Surowcami Mineralnymi / Mineral Resources Management, 25(3), 303–317.

Kuliczkowska, E. (2016). The interaction between road traffic safety and the condition of sewers laid under roads. Transportation Research Part D: Transport and Environment, 48, 203–213. https://doi.org/10.1016/j.trd.2016.08.025.

Kwiatek, J. (2007). Obiekty budowlane na terenach górniczych. Główny Instytut Górnictwa.

Lazecký, M., Rapant, P., Perissin, D., & Bakoň, M. (2014). Deformations of Highway over Undermined Ostrava-Svinov Area Monitored by InSAR Using Limited Set of SAR Images. Procedia Technology, 16, 414–421. https://doi.org/10.1016/j.protcy.2014.10.107.

Nosenzo, G., Whelan, B. E., Brunton, M., Kay, D., & Buys, H. (2013). Continuous monitoring of mining induced strain in a road pavement using fiber Bragg grating sensors. Photonic Sensors, 3(2), 144–158. https://doi.org/10.1007/s13320-012-0077-0.

Puertas, J. J. G. (2010). Estimating highway subsidence due to longwall mining (Vol. 9, Issue 1). https://doi.org/10.1558/jsrnc.v4il.24.

Rahman, M. S., & Erlingsson, S. (2015). Moisture influence on the resilient deformation behaviour of unbound granular materials. International Journal of Pavement Engineering, 17(9), 763–775. https://doi.org/10.1080/10298436.2015.1019497.

Rokitowski, P., & Grygierek, M. (2017). Wpływ niesprawnego odwodnienia na trwałość nawierzchni drogowej. In J. Bzówka & M. Łupieżowiec (Eds.), Analizy i doświadczenia w geoinżynierii (pp. 455–462). Wydawnictwo Politechniki Śląskiej.

Swarbrick, G., Meers, P., Lee Shoy, D., Kay, D., & Buys, H. (2015). Monitoring pavement relief of the Hume Highway during undermining. 657–670. https://doi.org/10.36487/acg_rep/1508_47_swarbrick.

The General Directorate for National Roads and Motorways. (2010). Wymagania Techniczne WT4 - Mieszanki niezwiązane do dróg krajowych.

Tong, L., Leo, L., Amatya, B., & Liu, S. (2016). Risk assessment and remediation strategies for highway construction in abandoned coal mine region: lessons learned from Xuzhou, China. In Bulletin of Engineering Geology and the Environment (Vol. 75, Issue 3, pp. 1045–1066). https://doi.org/10.1007/s10064-015-0760-7.

Tong, L., Liu, L., & Yu, Q. (2014). Highway construction across heavily mined ground and steep topography in southern China. Bulletin of Engineering Geology and the Environment, 73(1), 43–60. https://doi.org/10.1007/s10064-013-0503-6.

Zha, J., & Xu, M. (2019). High-grade highways deformation and failure laws in mining area–a case in Nantun Coal Mine, China. In International Journal of Pavement Engineering (Vol. 20, Issue 11, pp. 1251–1263). https://doi.org/10.1080/10298436.2017.1402592.

Zhang, D., Shen, N. Q., Li, X., Shu, Z. Y., & Xu, X. Le. (2013). Stability evaluation of highway near mined-out region. In Applied Mechanics and Materials (Vols. 361–363, pp. 1717–1722). https://doi.org/10.4028/www.scientific.net/AMM.361-363.1717.

ZSoil (2011) ZSoil manual, Elmepress and Zace Services Limited, Lausanne, Switzerland.